Annual Report 2009

Finite fault parameterization of intermediate and large earthquakes in Southern California and uncertainty analysis

Chen Ji (UCSB)

Finite fault parameterization of intermediate and large earthquakes in Southern California and uncertainty analysis

Seismologists generally expect that the improvement in observational conditions would lead to better source images. The station coverage of large earthquakes has been significantly improved as the recent quick implement of strong motion and broadband seismic networks globally, for instance, the networks in Taiwan, Japan and Southern California. Researchers would expect to have much better station coverage and more precise velocity structures during the studies of future earthquakes. However, a recent influent numerical exercise suggests that improving the surface station density only is not enough to solve the resolution problems.

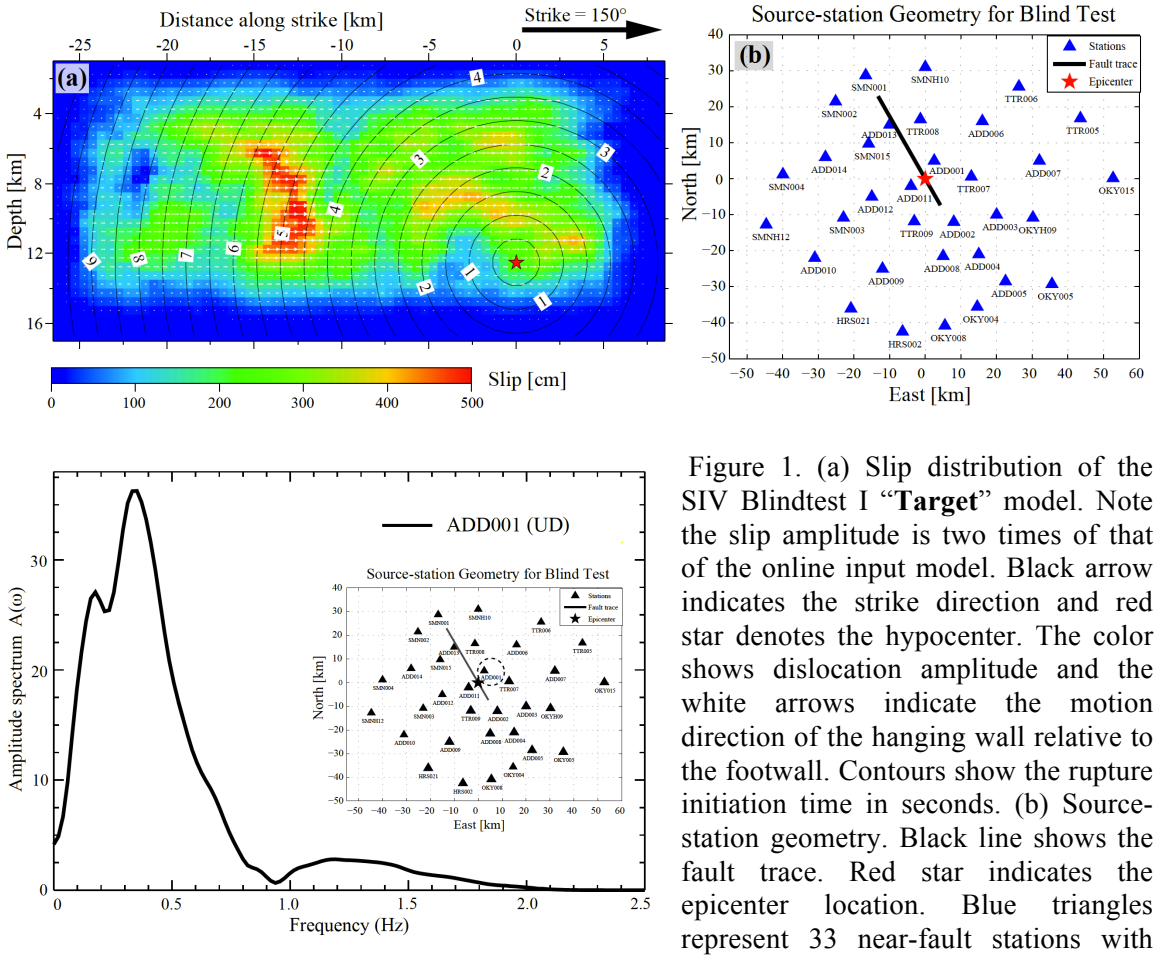

Figure 1. (a) Slip distribution of the SIV Blindtest I "**Target**" model. Note the slip amplitude is two times of that of the online input model. Black arrow indicates the strike direction and red star denotes the hypocenter. The color shows dislocation amplitude and the white arrows indicate the motion direction of the hanging wall relative to the footwall. Contours show the rupture initiation time in seconds. (b) Source-station geometry. Black line shows the fault trace. Red star indicates the epicenter location. Blue triangles represent 33 near-fault stations with station names below. (c) The amplitude spectrum of the vertical velocity record at the station ADD001. Note that most energy concentrates around the corner frequency of 0.33 Hz.

Aiming to understand the uncertainties of source inversion, Festa, Francois-Holden, and Mai launched the Source Inversion Validation (SIV) BlindTest within the framework of the SPICE (**S**eismic Wave **P**ropagation and **I**maging in **C**omplex Media: A **E**uropean Network) project in 2006. Researchers were encouraged to constrain the rupture process of a heterogeneous strike-slip rupture on a vertical fault, using noise-free synthetic data at a well distributed near-fault strong motion network

with a given velocity structure and fault geometry. Figure. 1a and 1b show the prescribed heterogeneous slip distribution of BlindTest 1, the fault geometry and the strong motion network composed of 33 stations. *Mai et al.* (2007) had reported the preliminary results of this problem from nine groups. The near ideal near-fault dataset and precise knowledge of the earth structure and fault geometry led to "***good"*** waveform fits, but not good inverted solutions. In particular, "*4 out of 9 inversion results are, statistically speaking, not better than a random model with somehow correlated slip*!" (Mai *et al.*, 2007). This counterintuitive result has influenced the opinions about earthquake source study in the geoscience community even since. One question cannot be escaped: if better station coverage and waveform fits than what we could achieve in practice cannot guarantee a reasonable recovery of the target model, should we trust any of previous source inversion results?

Table 1. Summary of frequency-dependent variance reductions and spatial cross-correlation associating wih different models

Models	*Variance reduction (%)*				*Spatial cross-correlation* S_{sc}
	BB *0-2(Hz)*	***LP*** *0.-0.1 (Hz)*	***DM*** *0.1-1.0(Hz)*	***SP*** *1.-2. (Hz)*	
Target	99.91	99.98	99.92	97.53	
Target_ST	99.32	99.72	99.43	86.12	1.0
Target_SC	99.32	99.72	99.45	86.21	1.0
Model I	99.35	99.28	99.61	77.02	0.972
Model I_BS	96.30	96.99	97.34	-0.34	
Model I_s	99.65	99.21	99.79	82.45	0.948
Model I_n1	50.01	57.62	59.16	14.21	0.970
Model I_n2	32.62	46.04	45.55	8.21	0.958
Model II	93.15	76.86	95.15	86.36	0.803
Model III	98.87	98.90	99.36	64.26	0.933

Target_ST: it is created by first dividing the fault plane of the **Target** into 1 km by 1 km subfaults and then assigning the slip amplitude of each subfault as the mean of the inside four grids. The rise time function is same as the target Model.
Target_SC: It is further modified from the model **Target_ST** by using a 0.9 s symmetric cosine function to replace the 0.8 s triangular slip rate function.
Model I: representative of the best inverted model using 1km by 1km subfaults and noise free data.
Model I_BS: representative of the best inverted model using 1.9 km by 1.9 km subfaults and noise free waveforms of 33 stations
Model I_s: similar to Model I but only 10 of 33 stations are used.
Model I_n1: similar to Model I but the data has been added Gaussian noise with a standard deviation of 5 cm/s.
Model I_n2: similar to Model I-n1 but the standard deviation of noise is equal to 35% of corresponding peak amplitude.
Model II: similar to Model I but he total seismic moment is forced to be half of the target.
Model III: similar to Model I but the peak slip is fixed to be half of the target.

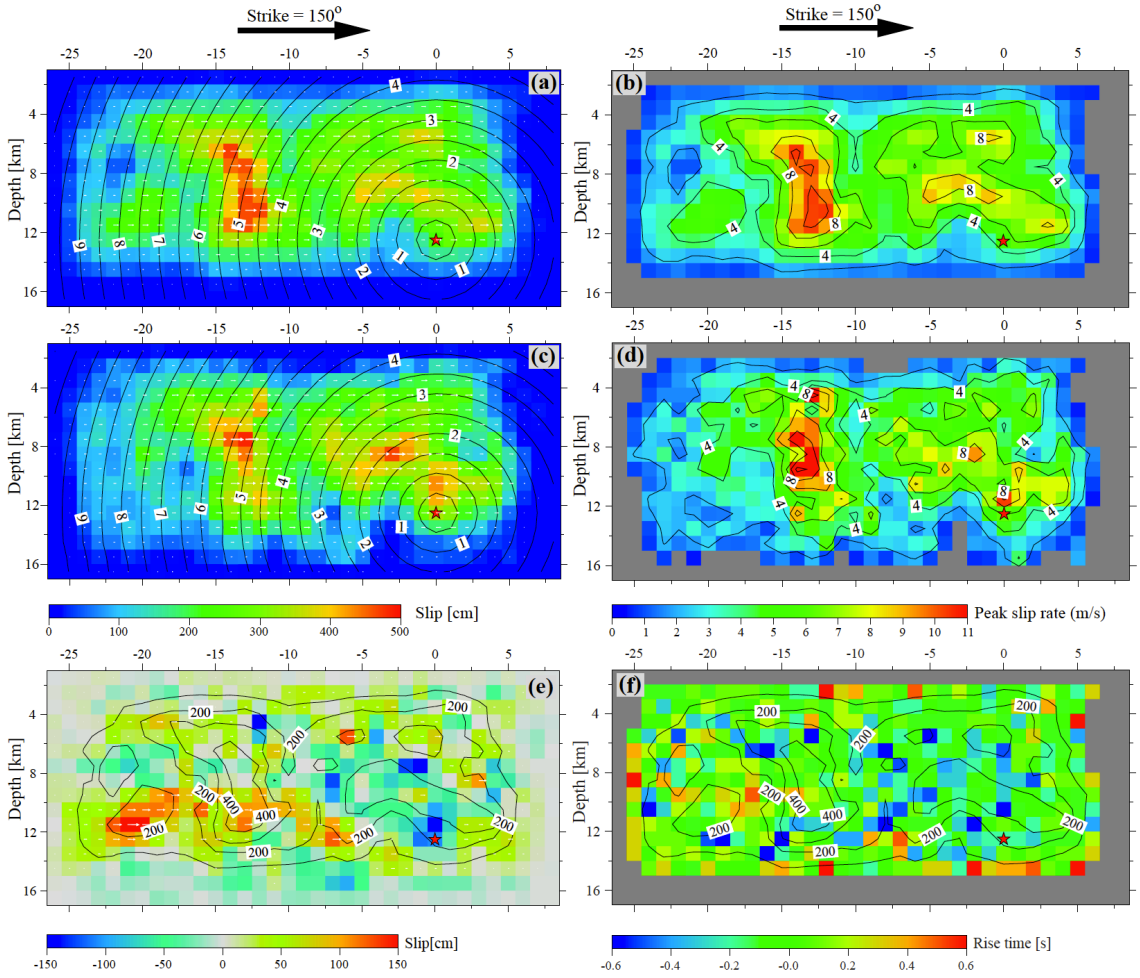

Figure 2. Comparison of slip and peak slip rate distributions of Model **Target_SC** and Model I. (a) and (c) show the slip distributions of model **Target_SC** (up) and model I. For each subfault, the color shows its dislocation amplitude and the arrow indicates the motion direction of the hanging wall relative to the footwall. Contours show the rupture initiation time in seconds. (b) and (d) show the corresponding peak slip rate distributions. Only the subfaults with a slip of 0.25 m or larger are presented here. (e) and (f) show the slip amplitude and rise time length difference between Model **Target_SC** and Model I. Contours are the slip amplitude of the **Target_SC** model in centimeters. The black arrow indicates the fault strike and the red star denotes the hypocenter location.

In response to these fundamental questions, we conducted a series of analyses to BlindTest 1. The objective function is the variance reduction between observed and synthetic velocity waveforms. Our studies reveal that first, the online dataset include a constant amplitude error. Second, even correcting this errors, the target model could be reasonably well but not fully recovered. Third, the inverted results are quite robust even the data includes large Gaussian noise. Fourth, the sensitivities to some basic source parameters are quite low. Models with good variance reductions could have erroneous total seismic moment and peak slip. Finally, we argue that other than the poor station coverage, inaccurate earth

structure and fault geometry, the following aspects could also result in significant uncertainties in the inverted solutions:

1. **The source parameterization affects the inverted results.** When we ignore the spatial variance within individual subfaults, the highest frequency of seismic signals that could be precisely modeled becomes limited. It then results in limitations in both the spatial and temporal resolutions. For instance, the Model target_SC, which is constructed by average the target model into 1 km by 1km subfault and is supposed to approximate the Target model best inside the model space, matches the data slightly worse than the inverted solution, Model I, in terms of overall variance reduction from 0 to 2 Hz (Table 1 and Figure 2).

2. **The model fitting the data in some frequency range usually does not suggest that it can predict the source spectrum at other frequencies**. Because the heterogeneous energy distribution in frequency as shown in Figure 1c, the standard objective functions tend to ignore the misfit in high frequency and therefore are suboptimal in extracting constraints embedded in the broadband seismic waveforms. Better objective functions, which include weight strategies to honor the characteristics of source spectrums and noise distributions, are crucial to take full advantage of extensive information embedded in seismic waveforms.

3. **The fits to the data or the values of objective functions cannot be used to evaluate the quality of the inverted model.** When we discuss whether the features of an inverted model are required by the data, further in-depth analysis must be preformed to estimate their uncertainties.

4. **The characteristics of earthquake focal mechanisms and seismic radiation affect the inverted result.** For instance, along strike slip variances of strike-slip rupture on a vertical fault are better resolved than the slip in the down-dip direction. The inversions using velocity records are more sensitive to the moment acceleration than the moment rate.

5. **All models summaried in Table 1 capture the general characteristics of the target BlindTest 1 model with a spatial cross-correlation larger than 0.8.** Readers should be cautious when they interpret the previous results of BlindTest 1.

Publication that resulted from our activity related to this project is

(1) Shao, Guangfu, C. Ji., *What Exercise of the SPICE Source Inversion Validation BlindTest 1 did not Tell You?* Journal of Geophysics International, submitted.

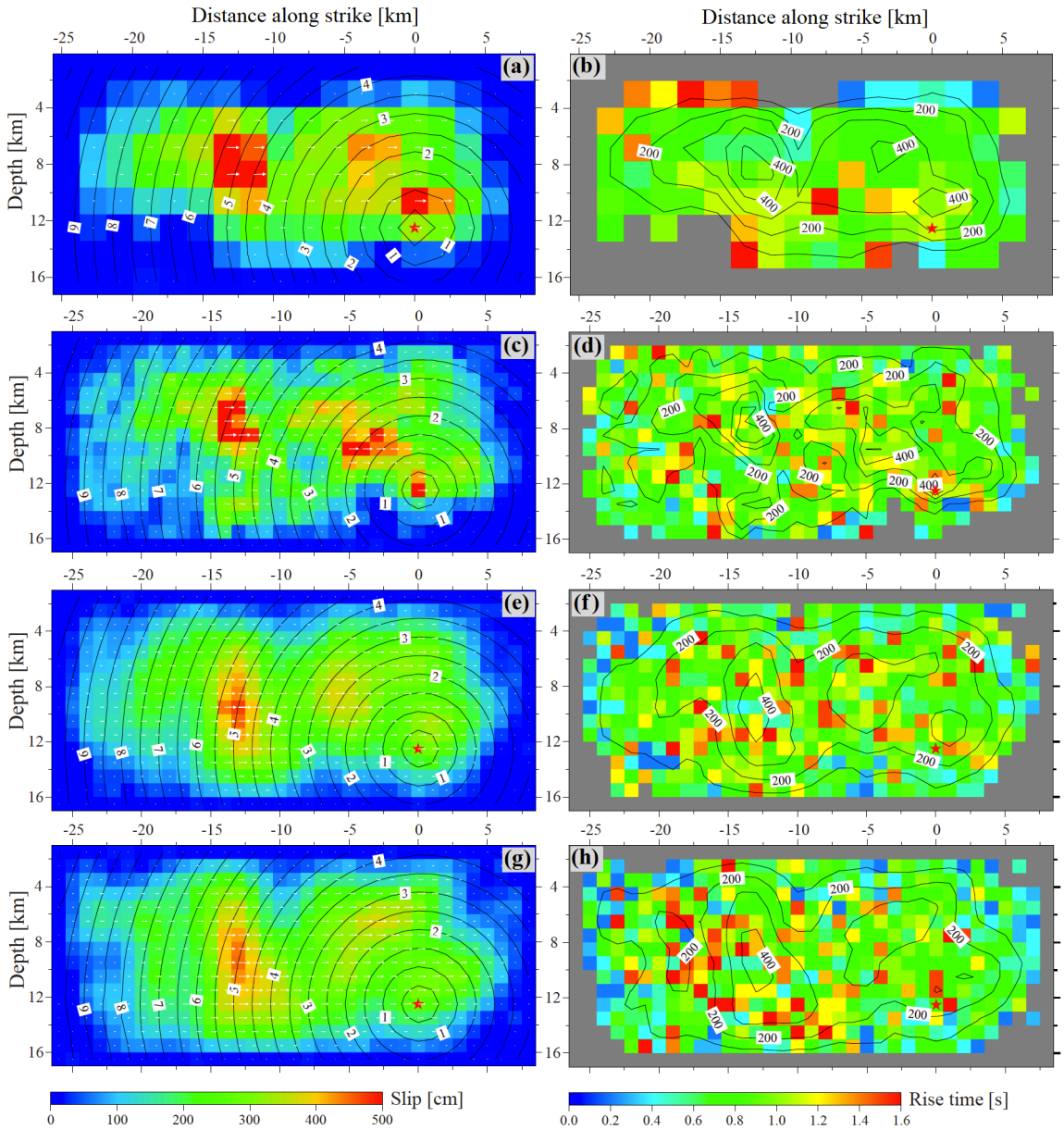

Figure 3. Comparison of slip and rise time distributions of Model **I_BS, I_s, I_n1 and I_n2**. Left panels show their slip distributions. Color indicates the dislocation amplitude and contours denote the rupture initiation time in seconds. Right panels show their rise time distributions. Color denotes width of slip-rate functions at the subfaults with slip amplitudes larger than 25 cm. Contours show the slip amplitude in centimeters. The black arrow indicates the fault strike and the red star shows the hypocenter location.

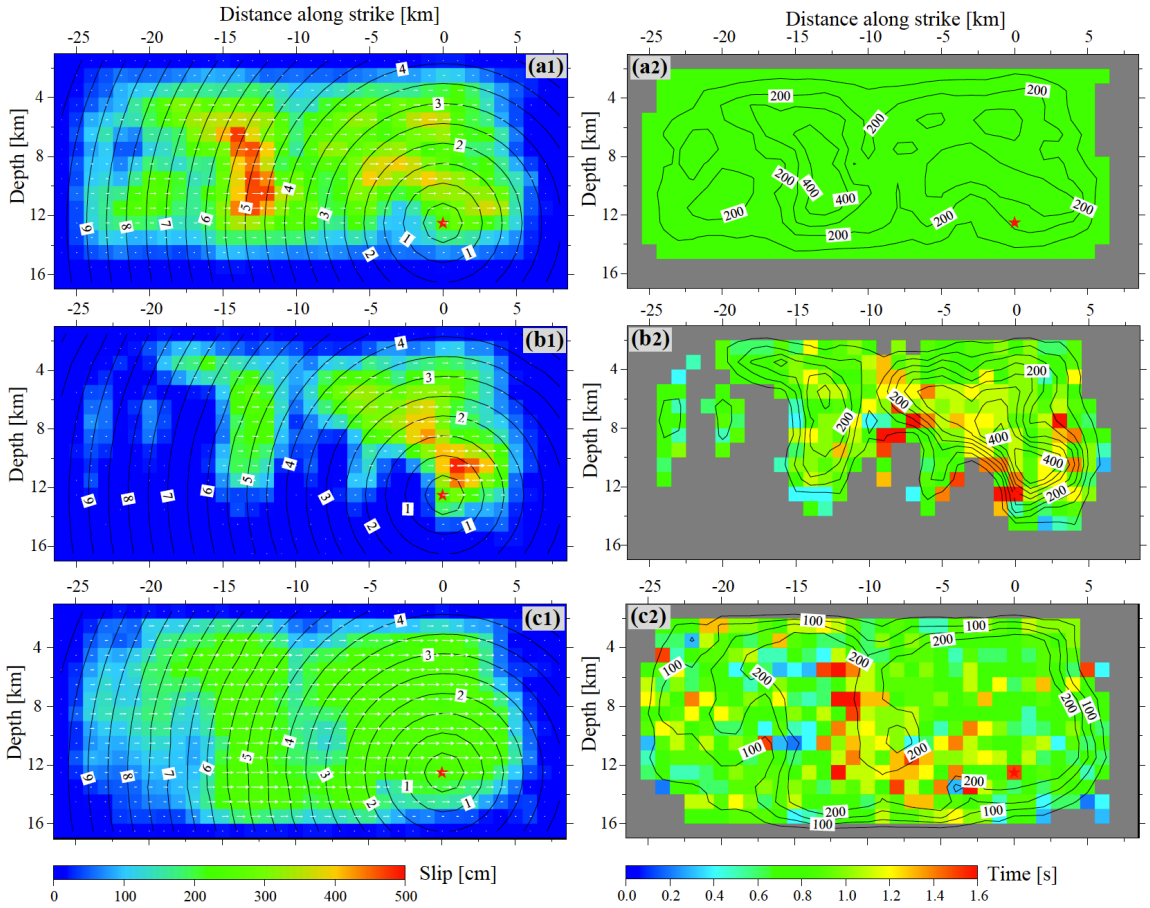

Figure 4. Comparison of inverted slip and rise time distributions on the cross sections. (a1), (b1) and (c1) show the vertical cross-sections of slip distributions of **Model Target_SC, II** and **III**, respectively. Color shows its dislocation amplitude and contours denote the rupture initiation time in seconds. (a2), (b2) and, (c2) show the corresponding rise time distributions. Color denotes the length of slip-rate functions at the subfaults with slip amplitudes larger than 25 cm. Contours show the slip amplitude in centimeters. The black arrow indicates the fault strike and the red star shows the hypocenter location.

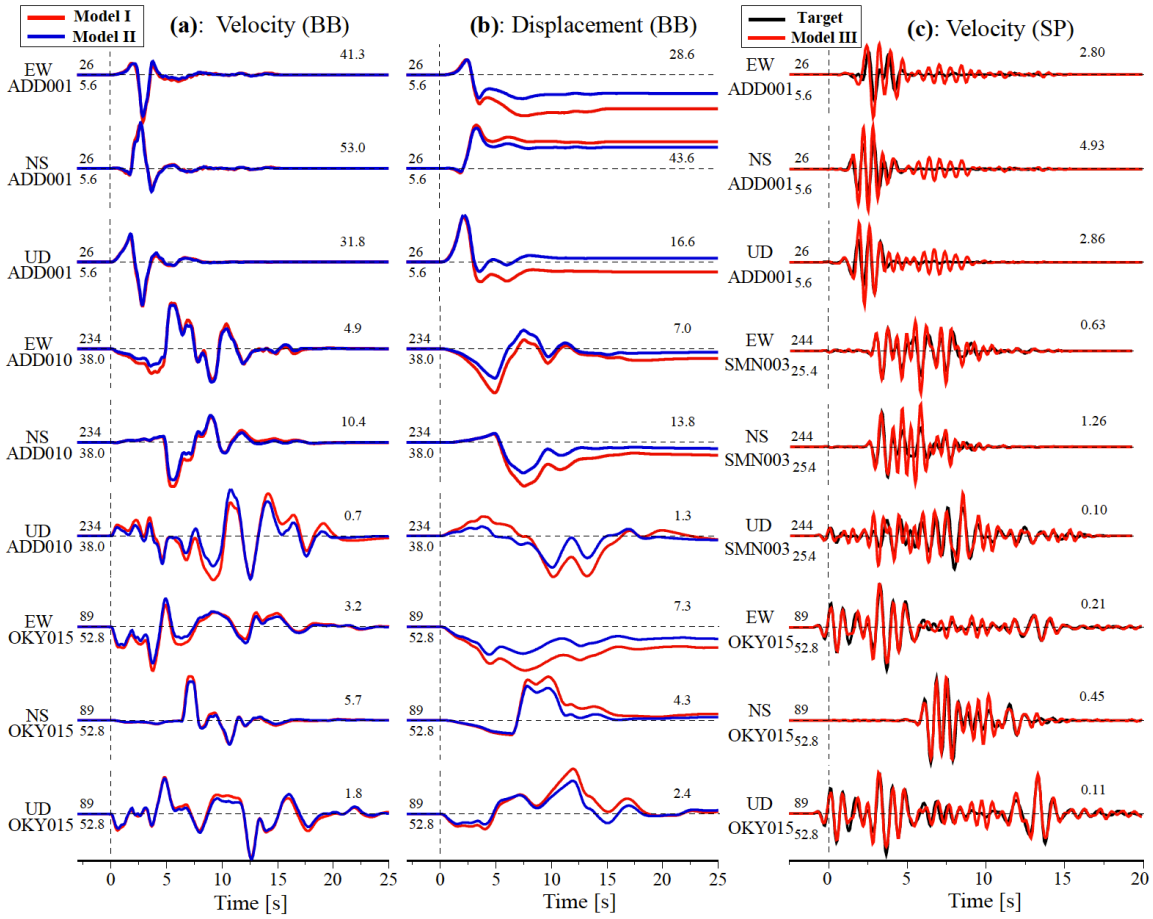

Figure 5. (a) Comparison of synthetic velocity waveforms of **Model I** (red lines) and **Model II** (blue lines) at three representative stations. All the seismograms are aligned on their P arrivals. The number above the beginning of each trace is the source azimuth in degrees and below is the epicentral distance in kilometers. The number at the end of each trace is the peak amplitude of the synthetics of **Model I**. (b) Comparison of synthetic displacements of **Model I** (red lines) and **Model II** (blue lines) at three representative stations, integrated from the synthetic velocity waveforms as shown in figure 11a. (c) Comparison of synthetic velocity waveforms of **Model III** (red lines) and the corrected data (black lines) in the SP band.